Dedicated spectrophotometer for localized transmittance and reflectance measurements

Laëtitia Abel-Tiberini, Frédéric Lemarquis, and Michel Lequime

A dedicated spectrophotometer is built to achieve localized transmittance and reflectance measurements. The spatial resolution can be chosen from 100 μm to 2 mm, the spectral resolution from 0.5 to 5 nm, and the spectral range from 400 to 1700 nm. This apparatus can be used to study the index and thickness uniformity on single layers to determine and optimize the characteristics of the deposition chamber. It can also be used to measure the spatial variations of optical properties of intended nonuniform coatings such as linear variable filters. © 2006 Optical Society of America

OCIS codes: 310.6860, 310.3840.

1. Introduction

Transmittance and reflectance measurements are frequently used in the thin-film field either to measure the optical properties of coatings or to characterize the refractive index and thickness of single layers.[1] In this last case, and provided that several substrates are coated at the same time, the goal can be the characterization of the thickness uniformity of the deposition chamber.[2–5] Usually these measurements are performed with spectrophotometers that have a beam diameter of typically several millimeters, and results that are obtained by using such illumination conditions are in fact values averaged over the analysis surface. Such results can be accepted in most cases; however, for some specific applications, such a measurement area is too large and there is a need for localized measurements with a better spatial resolution. This is obviously the case for all components with lateral dimensions smaller than the beam diameter. For example, dense-wavelength-division-multiplexing (DWDM) coatings can be characterized with a classical spectrophotometer, but since the size of DWDM filters is ~1 mm, specific measurement devices must be developed. Moreover, because such filters are known to require a high thickness uniformity, the thickness distribution must be master, and consequently studied, with a spatial resolution smaller than 1 mm. Intended-nonuniform filters, such as linear variable filters,[6] also provide an example in which classical spectrophotometers can rarely be used. For such filters, coatings are manufactured with a thickness gradient along one direction, which allows one to obtain a large wavelength shift in the optical properties along this direction. This kind of filter is of great interest to the manufacture of small, light, and compact spectrometers. Typically, along the 1 or 2 cm corresponding to the size of the component, the center wavelength can increase by a factor of 2. Here again, the thickness distribution must be controlled and studied properly with a spatial resolution smaller than 1 mm. Since these coatings are highly nonuniform, they cannot be measured with a large spot diameter owing to the wavelength shift that occurs across the beam diameter. Here again, specific measurement capabilities must be developed, but contrary to DWDM filters, which need only to be studied on a short spectral range (~1550 nm) that can be provided by a tunable laser, linear variable filters must be measured over a wide spectral range.

To resolve these difficulties, we decided to develop a specific measurement bench that allows both localized transmittance and reflectance measurements. This apparatus operates in the visible and near-infrared spectral ranges with several calibrated values for the beam diameter, extending from a few tenths to a few millimeters. Moreover, the sample holder is motorized with two translation stages to

The authors are with the Institute Fresnel, Unité Mixte de Recherche, Centre National de la Recherche Scientifique 6133, Université Paul Cézanne, Domaine Universitaire de Saint Jérôme, 13397 Marseille cedex 20, France. L. Abel-Tiberini's e-mail address is laetitia.abel@fresnel.fr.

Received 28 February 2005; revised 27 July 2005; accepted 10 August 2005.

0003-6935/06/071386-06$15.00/0

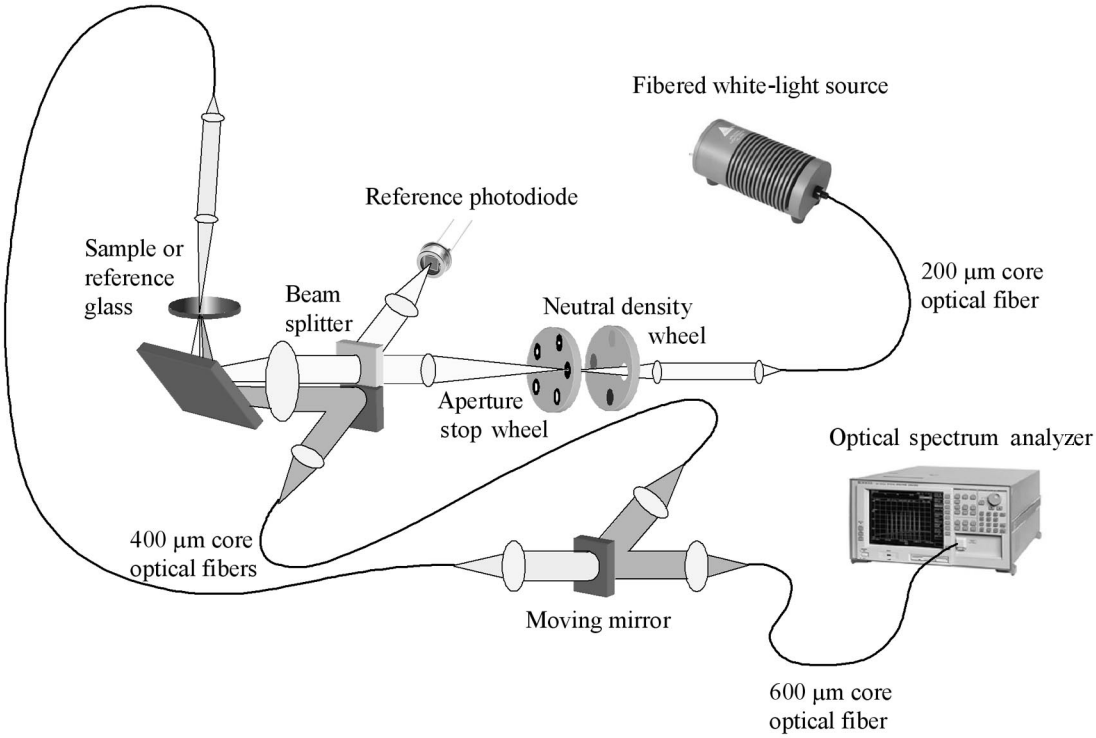

Fig. 1. Schematic representation of the spectrophotometer.

perform automatic two-dimensional (2D) mappings of the coatings.

Section 2 is devoted to the physical description of this bench. Then we study its technical data and measurement performances. Finally, we illustrate the application of the apparatus to the thickness-distribution characterization and to the measurement of a linear variable filter.

2. Physical Description of the Spectrophotometer

The principle we use to obtain a precisely localized analysis surface is to form on the sample the geometrical image of a calibrated aperture stop, as is shown in Fig. 1. Following the propagation of light, we place this aperture stop in front of the sample, which allows us to control visually the probing-zone location on the sample. Several aperture stops of different diameters, all located on a wheel, are available, permitting the adaptation of the spatial resolution according to the kind of measurement we want to perform. Obviously, selecting a small analysis surface to improve the spatial resolution decreases the flux level and consequently the signal-to-noise ratio.

At the entrance of the system, the light source is imaged on the aperture stop while, at the exit of the system, the sample is imaged on the entrance slit of a monochromator either by way of the reflected beam or by way of the transmitted beam.

Now both the light source (quartz halogen) and the monochromator (optical spectrum analyzer ANDO AQ 6315-A) are connected to the bench by means of optical fibers. This configuration gives the setup more flexibility. Another advantage is that the illumination exiting from the entrance fiber can be considered fully uniform (within 5%). As a consequence, the sample and the aperture stop are in fact imaged on the entrance and exit planes of these fibers, respectively. Moreover, assuming that a single fiber is used between the sample and the monochromator, this fiber should be moved or disconnected each time we want to perform either a reflectance or a transmittance measurement, something that is not conducive to signal stability. To avoid this difficulty, we used two fibers, one for each measurement channel, and by means of a motorized switch mirror coupled each of these intermediate fibers to a third one, which is connected to the monochromator.

Notice that for easier alignment, the core-fiber diameters are increased along the setup. The entrance- and exit-fiber diameters are, respectively, 200 and 600 μm, while the diameter of the two intermediate fibers used for the reflectance and the transmittance channels is 400 μm. All these fibers are step-index fibers with identical numerical apertures.

However, the optical conjugation between these fibers is not a sufficient condition to completely transfer the light from one optical fiber to the next, since we must also preserve the angular distribution of the beam. For this purpose, all image formations are performed by means of two-lens telecentric objectives.

Magnification ratios are equal to 10, 1, 1/10, and 1 between the entrance fiber and the aperture stop, the aperture stop and the sample, the sample and the intermediate fibers, and the intermediate fibers and the exit fiber, respectively. Consequently, the largest measurement area, in the absence of any

aperture stop, is a 2 mm wide diameter, owing to the diameter of the entrance fiber.

To complete the physical description, notice that we include a beam splitter (in fact a glass substrate) to feed a reference photodiode that allows to correct measurements from fluctuations of the light source intensity. Finally, for a more-convenient handling of the samples, we decided to design a horizontal sample holder on which the sample and a reference glass can be positioned side by side. The transmission measurement is thus performed vertically. The substrate holder is motorized along two axes in the horizontal plane so that we can perform 2D mappings of the samples.

3. Technical Characteristics and Performance

Concerning geometrical characteristics, due to the numerical apertures of the optical fibers and to the magnification of the system, the divergence of the measurement beam on the sample is 1.25 deg. The mean incidence angle on the sample is ~2 deg.

The diameters available for calibrated apertures and the consequent measurement areas are 100, 200, 600, and 1000 μm. As mentioned before, the beam diameter on the sample is 2 mm when no aperture stop is used. Notice that, due to absorption or scattering, the presence of dust or defects on either the sample or the reference glass can rapidly falsify the results as the probing-zone diameter is decreased.

Displacements of the sample holder are performed by stepper motors. The maximum displacement along the direction defined by the sample and the reference glass is 60 mm. The maximum displacement along the perpendicular direction is 25 mm. The displacement accuracy is 3 μm.

Concerning the spectral characteristics, measurements are performed with an optical spectrum analyzer (ANDO AQ 6315-A). The spectral range extends from 400 to 1700 nm. The spectral resolution depends on the diameter of the optical fiber that is connected to the apparatus since this optical fiber serves as the entrance slit. In the best case (i.e., using a monomode fiber) the spectral resolution is 0.05 nm. In our case (i.e., using a 600 μm optical fiber) the spectral resolution is 5 nm. To improve the spectral resolution, we thus need to use smaller values for the fiber-core diameters, which first tend to reduce the positioning tolerances for the bench alignment. For this purpose, a 100 μm diameter optical fiber is also available to connect the optical spectrum analyzer, which gives a 0.5 nm spectral resolution. Associated with this 100 μm fiber are two 50 μm diameter intermediate optical fibers for the reflection and transmission channels. However, notice that, due to the magnification of the objectives that are used to image the sample on the intermediate fibers, the diameter of the probing zone cannot exceed 500 μm. As one can see, improving the spectral resolution not only reduces the positioning tolerances but automatically reduces the size of the measurement area and consequently the flux level. However, if the sample needs to be measured through a small probing diameter, owing to a large nonuniformity of the coating, for example, as is the case of linear variable filters, the spectral resolution can be improved without increasing flux losses.

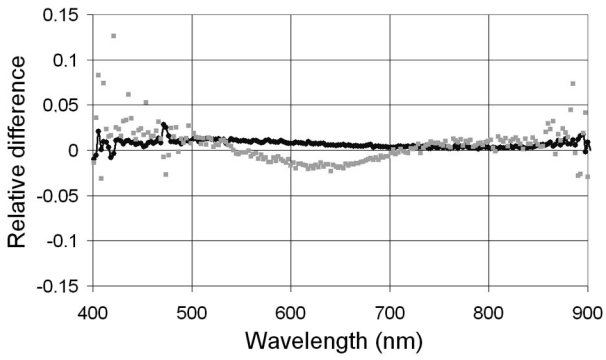

Fig. 2. Relative difference of the transmittance (solid curve) and the reflectance (gray curve) measured for a single high-index level on a Lambda 18 PerkinElmer spectrophotometer and on our measurement bench.

According to the flux level, the optical spectrum analyzer automatically adjusts the integration time. For our operating conditions, the measurement of one point over the whole spectral range from 400 to 1700 nm takes ~60 s under the most favorable conditions (namely, for a 2 mm beam diameter), while it requires ~360 s for a 100 μm beam diameter.

Regarding the measurement performance, we first considered the evolution of the signal over 2 h to estimate the relative stability of the system, including both the stability of the light source and that of the optical spectrum analyzer. For a 2 mm probing zone, we found that the standard deviation is $\sim 10^{-4}$. Then we considered a set of 200 measurement cycles, including each time the measurement was made through the sample and through the reference glass. These measurements were performed with a 1 mm probing zone and, to estimate the repositioning repeatability, the sample was replaced by another 1 mm calibrated aperture stop centered on the probing zone. Taking into account the flux variation of the light source by means of the reference photodiode, the results showed that the measurement repeatability, including the sample displacements, is $\sim 10^{-3}$.

At last we compared the measurements given by this apparatus with the results given by the PerkinElmer Lambda 18 spectrophotometer that is available in our laboratory, for which the spectral range extends from 180 to 850 nm. As a consequence, results could be compared only between 400 to 850 nm. The sample used for this comparison was a HfO_2 single-layer, 160 nm thick sample deposited on a silica substrate. Figure 2 gives the relative differences in the transmittance and reflectance measured with the two spectrophotometers, which correspond to the following quantities:

$$2(T_{PE} - T)/(T_{PE} + T), \quad (1)$$

$$2(R_{PE} - R)/(R_{PE} + R), \quad (2)$$

where T_{PE} and T represent the transmittance measured with the PerkinElmer spectrophotometer and with the spectrophotometer we developed, respectively. Similar notations are used for the reflectance.

Note that for this example the spot diameter of our setup is 2 mm, whereas it is ~5 mm for the PerkinElmer spectrophotometer. For the major part of the spectrum, namely between 500 and 850 nm, the relative difference is less than ±0.01. Noise between 400 and 500 nm is due to the low flux level of our halogen source at these wavelengths. On the contrary, the noise observed beyond 850 nm is due to the limited spectral range of the Lambda 18 spectrophotometer.

Finally, the difference between the losses measured by these two apparatus types remain lower than 1.5×10^{-2}. Notice that neither apparatus is capable of discriminating between losses from absorption and those from scattering. In conclusion, the performances of the measurement bench we developed are as good as those given by commercial spectrophotometers that are classically used for coating characterization.

At last the spectrophotometer is completely automated, which is convenient for 2D mappings on coatings. In such cases, according to the density of the spatial grid that is used, the total measurement time can easily exceed 10 h, and we observed a slight variation in the signal over this time period although the measurements were corrected from the light-source fluctuations by means of the reference photodiode. This indicates that other parts of the bench (most likely the optical spectrum analyzer) are not stable enough for such long measurement durations. To avoid this problem, we performed a periodic calibration of the bench by measuring the reference glass every 3 h. This procedure allows us to maintain measurement accuracy.

4. Applications

To illustrate the capabilities of this spectrophotometer, we give in this section two examples. The first one corresponds to the thickness-uniformity characterization of a single layer (Subsection 4.A), and the second one to the measurement of the optical properties of a linear variable filter (Subsection 4.B).

A. Single-Layer Thickness Uniformity

The sample that is considered in this subsection is a Ta_2O_5 single layer deposited on a silica substrate by dual-ion-beam-deposition sputtering (DIBS). The sample's optical thickness is approximately 6H, where H corresponds to a quarter-wave layer at a wavelength of 1550 nm. The diameter of the coated surface is ~21 mm. The mapping is composed of $20 \times 20 = 400$ points distributed on a regular square grid, using a step equal to 1100 μm. For each point, the reflectance and transmittance were measured with a beam diameter of 600 μm and a spectral resolution of 5 nm. The total measurement time was 30 h.

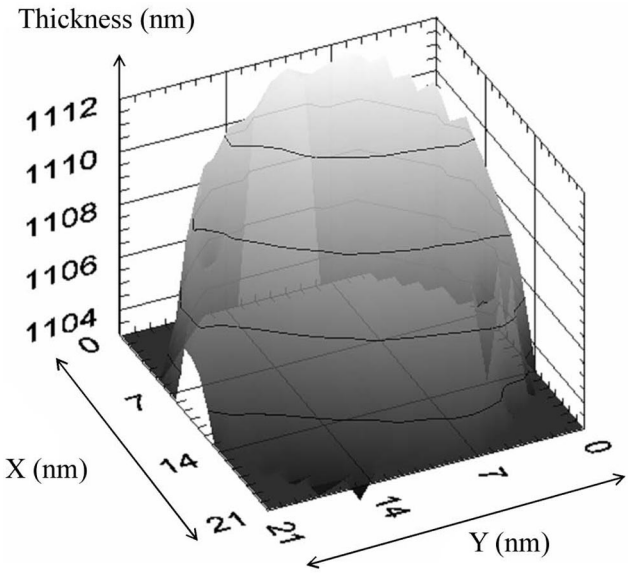

Fig. 3. Thickness distribution measured on a high-index single layer. Maximum thickness is 1111 nm. Isothickness lines are drawn every 2 nm.

After measurement, we extracted the mechanical thickness and refractive index separately for each point. Except for a few points for which obviously the result is not correct, the index standard deviation is $\sim 1 \times 10^{-3}$, for a mean index value of 2.089 at a wavelength of 1550 nm. This means that nonuniformity concerns mainly the film's mechanical thickness. Figure 3 gives a representation of the mechanical film thickness over the sample surface. Each solid curve represents a variation of 2 nm. The maximum thickness is equal to 1111 nm. The uniformity of the sample is ~1%.

More generally, notice that the precision of the index and thickness determinations strongly depend on the signal-to-noise ratio. To estimate this point, we performed numerical simulations of the index determination, considering an additive noise on both the reflectance and the transmittance profiles. For these tests, the layer was assumed to have a 2.1 refractive index and a 1142 nm thickness, and the optical properties were calculated for 900 wavelengths between 550 and 1650 nm. We used 400 random distributions for each noise level. The final result is that the standard deviation of the refractive index is proportional to the standard deviation of the noise added to the reflectance and transmittance profiles, which is approximately equal to one tenth of this value in our case: $\sigma_{\text{ref index}} = \sigma_{\text{opt prop}}/10$. Notice that this ratio depends strongly on the thickness of the layer as well as on the index mismatch among the layer, the substrate, and the external medium.

In any case, this result shows that the signal-to-noise ratio must be correct to reach a given refractive-index accuracy. In particular, assuming that the signal ratio is proportional to the measurement area, that is to say proportional to the square diameter of the beam, it is necessary to compensate the flux re-

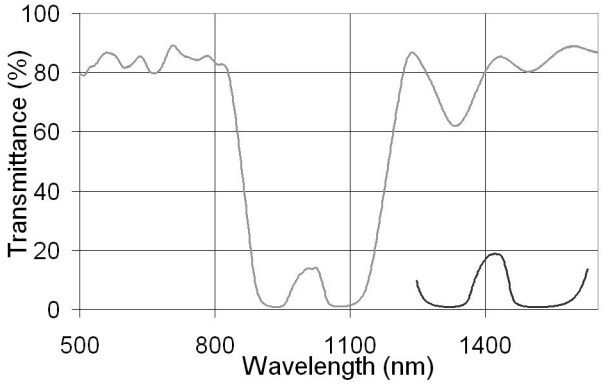

Fig. 4. Transmittance measured on two points of a linear variable filter with a 2 mm surface analysis and a 5 nm spectral resolution. The wavelength shift across the probing zone prohibits a correct measurement of the bandpass of the filter.

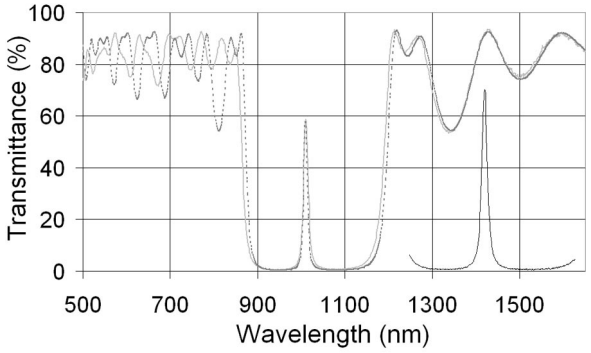

Fig. 5. Transmittance measured (solid curve) on two points of a linear variable filter with a 200 μm surface analysis and a 5 nm spectral resolution. For the leftmost peak, the dashed curve corresponds to the calculation of the transmittance profile, taking into account spatial and spectral integration.

duction due to the selection of a small aperture by an increase in the integration time in order to maintain measurement quality. This can rapidly result in a prohibitively long measurement period (36 h for the example we present here), and some compromise must be made among the expected index accuracy, the spatial resolution, and the spatial grid used for mapping.

By using such measurements, our spectrophotometer is helpful for characterizing and optimizing the thickness distribution of deposition chambers.

B. Linear Variable Filter

As mentioned in Subsection 4.A, the bandpass coating that is considered in this subsection was manufactured by DIBS, using Ta_2O_5 and SiO_2 as layer materials. This coating is formed by a single-cavity Fabry–Perot design, using 10 quarter-wave layers for each mirror and a 4H spacer layer in between. The center wavelength of this design goes approximately from 800 to 1600 nm from one side of the substrate to the other. The substrate is square in shape, 20 mm on each side. For such a filter, a large wavelength shift in the optical properties can be observed along the direction of the thickness gradient. As a consequence, the measurement of the optical properties cannot be performed with a large probing diameter since the result will correspond to an integrated value across this diameter. This is illustrated in Fig. 4, which gives the transmittance measured on two points 9 mm apart, using a probing diameter of 2 mm and a spectral resolution of 5 nm. For these points, the center wavelengths are 1010 and 1420 nm, respectively, and the maximum transmittance does not exceed 20%, while it should be 96%, and the width of the bandpass at half-maximum is ~50 nm, while it should be ~7 nm, considering a uniform filter or a pinpoint measurement.

Figure 5 gives the corresponding results, this time using a probing diameter of 200 μm and a spectral resolution of 5 nm. As expected, the results are much better, although they still do not reach the theoretical performance of the uniform filter. For one measured point, as a comparison, Fig. 5 also gives the calculated transmittance, taking into account both the spatial integration over the circular probing zone and the spectral resolution. For this calculation, the thickness gradient was assumed constant and was evaluated with known center wavelengths measured for these two points and a known distance between these points. As one can see, the agreement between the measurement and the calculation is excellent, except for the left-hand-side transmitted band, which is probably due to manufacturing thickness errors. Notice that in Fig. 5 the maximum transmittance of the bandpass is lower at 1010 nm than at 1420 nm. Again, this phenomenon is due to the integration over the probing zone and to the fact that the bandwidth of the filter is shorter at 1010 nm than at 1420 nm. A complementary phenomenon can be observed upon reflection, as can be seen in Fig. 6. Notice that measurements upon reflection are quite noisy for a high reflection level, owing to the low flux level measured for calibration on the silica substrate used as a reference glass, and the use of a small probing zone. However, these measurements permit us to confirm both experimentally and theoretically that the de-

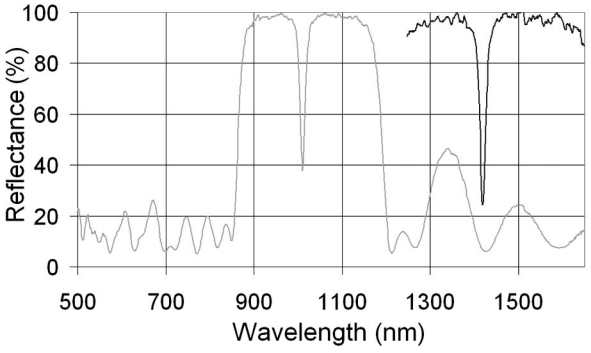

Fig. 6. Reflectance measured on two points of a linear variable filter with a 200 μm surface analysis and a 5 nm spectral resolution.

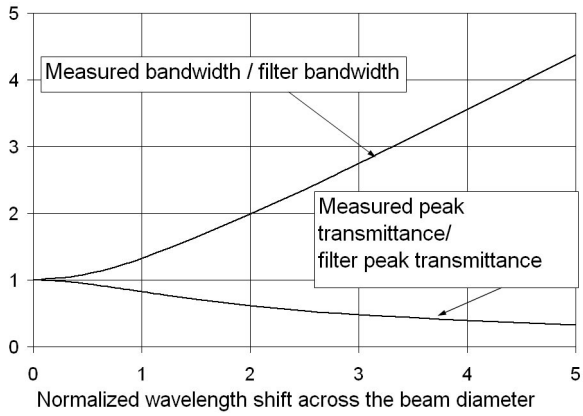

Fig. 7. Evolution of the measured peak-transmittance bandwidth (normalized to the ideal filter characteristics) versus the normalized wavelength shift $\Delta\lambda_{beam}/\Delta\lambda_{filter}$ due to nonuniformity across the beam diameter. The calculation is performed for a single-cavity bandpass filter.

crease in transmittance toward shorter wavelengths is not due to absorption.

More generally, the relevant parameter used to estimate the deviation of the filter characteristics from its ideal ones, which corresponds to a pinpoint measurement, is the ratio $\Delta\lambda_{beam}/\Delta\lambda_{filter}$ between the wavelength shift across the beam diameter $\Delta\lambda_{beam}$ and the bandwidth of the filter $\Delta\lambda_{filter}$. For a single-cavity Fabry–Perot filter, Fig. 7 gives the evolution of the measured bandwidth (normalized by the ideal bandwidth $\Delta\lambda_{filter}$) as well as the evolution of the maximum transmittance of the peak (normalized by the ideal maximum transmittance). As expected, significant modifications occur as soon as the wavelength shift that is due to nonuniformity exceeds the bandwidth of the filter. A similar curve can be drawn to illustrate the effect of the spectral resolution used for measurements since the phenomenon is about the same. Notice that in the case of linear variable filters, the bandwidth of the filter is proportional to its center wavelength and consequently decreases toward shorter wavelengths, whereas the spectral shift across the beam diameter, as well as the spectral resolution used for measurement, is constant. This explains why the measured spectral profile is more affected in the spectral region corresponding to the shorter wavelengths. All kinds of coatings, including edge filters, might be affected by such modifications when their spectral response contains abrupt variations compared with the spectral shift due to nonuniformity.

In any case, even if the measurement area should be further reduced, which is not realistic because the corresponding flux reduction would rapidly decrease the measurement quality, our spectrophotometer gives us results that are sufficiently accurate to develop a correct interpretation of the coating characteristics. Associated with the 2D mapping presented in the above example, we can perform a complete characterization of an intended nonuniform filter to determine, for example, the thickness gradient, its orientation, or the shape of the isothickness lines. This point is particularly important for linear variable filters that must be associated with a 2D matrix detector. Indeed, for such filters the uniformity that is perpendicular to the main thickness gradient should be as high as possible so that each column of the detector is assigned a single wavelength. Such results are of great relevance to the optimization of the masking technique used in the manufacture of such components.

5. Conclusion

In this paper we described the spectrophotometer that we developed to perform localized reflectance and transmittance measurements. The spectral range of the spectrophotometer extends from 400 to 1700 nm. Using the largest probing zone, namely, 2 mm in diameter, we achieved a radiometric performance with this apparatus that is similar to that of commercial spectrophotometers classically used for thin-film characterization. The main limitation of our apparatus concerns its spectral resolution, which is most often equal to 5 nm. However, the major interest of this apparatus is that the probing-zone diameter can be reduced to $\sim$100 μm, still preserving an acceptable measurement quality and permitting us to characterize microfilters or, with respect to 2D mapping capabilities, to characterize thickness uniformity or highly nonuniform coatings. At present, a major improvement would entail changing the light source for a new one with a higher radiance, such as a xenon arc lamp.

With our apparatus, we are now able to characterize accurately and with a high spatial resolution the thickness distribution of our deposition chambers. This will provide us with the entrance data needed to simulate the deposition process, which will allow us to optimize the mask shape and movements that are necessary to master the coating uniformity for the manufacture of highly uniform coatings or of linear variable filters with the prescribed thickness gradients.

References

1. J. P. Borgogno, B. Lazaridès, and E. Pelletier, "Automatic determination of the optical constants of inhomogeneous thin films," Thin Solid Films **102,** 209–220 (1983).
2. C. Grèzes-Besset, "Uniformity in thin-film production," in *Thin Films for Optical Systems,* F. Flory, ed. (Marcel Dekker, 1995), pp. 249.
3. C. Grèzes-Besset, F. Chazallet, G. Albrand, and E. Pelletier, "Synthesis and research of the optimum conditions for the optical monitoring of non-quarter-wave multilayers," Appl. Opt. **32,** 5612–5618 (1993).
4. F. Villa and O. Pompa, "Emission pattern of real vapour sources in high vacuum: an overview," Appl. Opt. **38,** 695–703 (1999).
5. F. Flory, E. Pelletier, G. Albrand, and Y. Hu, "Surface optical coatings by ion assisted deposition techniques: study of uniformity," Appl. Opt. **28,** 2952–2589 (1989).
6. A. Piegari, "Metal/dielectric coatings for transmission filters with wide rejection bands," in *Advances in Optical Thin Films,* C. Amra, N. Kaiser, H. A. Macleod, eds., Proc. SPIE **5250,** 343–348 (2003).